



Regular article

Temperature profile guided segmentation for detection of early subclinical inflammation in arthritis knee joints from thermal images

Mrinal Kanti Bhowmik^{a,*}, Kakali Das^a, Debotosh Bhattacharjee^b^a Department of Computer Science and Engineering, Tripura University, Suryamaninagar, Tripura, 799022, India^b Department of Computer Science and Engineering, Jadavpur University, Kolkata, West Bengal, India

ARTICLE INFO

Keywords:

Hotspot detection
Inflammation
Region growing
Thermal imaging

ABSTRACT

In arthritis, subclinical inflammation referred to the clinical condition when rheumatologists are in confusion about the presence of inflammation using clinical and pathological observations. Application of Thermal imaging in detection of subclinical inflammation is highlighted in this literature. Segmentation of the hotspot area from the thermal image is the initial step for further analysis of the hotspot. Analysis of the hotspot will help in prediction of the subclinical inflammation, impact of inflammation. Methodologies reported in existing literature for segmentation of hotspot or inflamed knee region in medical thermal images suffer from over and under extraction.

In the present scope, we try to overcome this limitation by extending the conventional region growing segmentation technique with stronger similarity criteria and stopping rule. In this method, hotspot or inflamed region is generated by taking the intersection of two independent regions produced by two different version of Region growing algorithm using a separate set of parameters. An automatic multiseed selection procedure ensures prevention of missed segmentation. We validate our technique by experimentation on various thermal image datasets like a newly created inflammatory thermal knee-joint-Database of 50 images, DBT-TU-JU Dataset, and DMR-IR Dataset. The effectiveness of the proposed technique is established compared to the performance of state-of-the-art competing methodologies.

1. Introduction

Diseases cause inflammation of joints known as arthritis. Single or multiple joints may get affected [1] in arthritis. Pain and swelling in joints, stiffness of joints, restriction of movements of joints are common symptoms of arthritis [2]. Arthritis causes joint destruction which produces inflammation in the proximity of that joint. Rheumatologist plan the treatment for arthritis patients based on the inflammation as it can describe the activity of related disease. Reduction in inflammation of joints indicates the decrease in the progression of disease [3–5]. Subclinical inflammation is an important issue to be considered in the treatment of arthritis.

Subclinical inflammation is referred to the clinical condition when rheumatologists unable to predict the presence of inflammation [8]. Presence of Inflammation is detected by Rheumatologists using clinical and pathological examination. Swelling, tenderness, pain, restriction of movements and temperature in joint surface are the clinical parameters consider to diagnosing the inflammation. Blood markers such as C-Reactive Protein (CRP) and Erythrocyte Sedimentation Rate (ESR) are the

pathological tool for inflammation diagnosis. The condition of subclinical inflammation arises when clinical and pathological observations contradict. Imaging technologies are also used for better understanding of early subclinical inflammation such as ultrasonography (USG), magnetic resonance imaging (MRI) [6,7]. But these modalities are costly and observer dependent. Among them MRI persists radiation during examination. The distant goal of this paper is to provide an alternative opinion to the clinicians (radiologists, rheumatologists, etc.), who may feel confused about the possible presence of subclinical inflammation in knee joint arthritis.

In this scope, the paper signifies the importance of thermal imaging towards diagnosis of subclinical inflammation. Every object including human body maintains an inherent temperature profile and change in that profile usually indicate an abnormality [9]. Thermal medical imaging is able to detect the difference in the temperature profile of the concerned area of skin surface. The increase of temperature in the affected area reflects as a hotspot or inflamed region in thermal images [13,14]. Therefore, thermal images of arthritis patients with a hotspot confirm the presence of inflammation. As the hotspot contains

* Corresponding author at: Computer Science and Engineering Department, Tripura University (A Central University), 799022, India.

E-mail address: mrinalkantibhowmik@tripurauniv.in (M.K. Bhowmik).

<https://doi.org/10.1016/j.infrared.2019.04.011>

Received 12 January 2019; Received in revised form 10 April 2019; Accepted 10 April 2019

Available online 11 April 2019

1350-4495/ © 2019 Elsevier B.V. All rights reserved.

Table 1
Details of some case study of subclinical findings on over small dataset of arthritis patients.

Sl No.	Patient_id	Diseases	Duration	Effectted joint	ESR	CRP	Pain	Synovities	Swelling	Tenderness
1	6	Reactive Arthritis	5 Month	Left Knee	81	7	Mild	No	mild	mild
2	19	Mono-Arthritis	5 Month	Knee	65	6.9	Mild	No	mild	nil
3	21	Osteo-Arthritis	1 Year	Left knee	50	1.4	Moderate	Not confirmed	moderate	mild
4	27	Osteo-arthritis	1 Months	Both knee	65	7	Moderate	Not confirmed	moderate	moderate
5	28	Osteo-arthritis	1 Months	Right Ankle	50	6.0	Severe	Not confirmed	Severe	Severe
6	35	Osteo-arthritis	1 Year	Left Knee	60	Neg	Moderate	Not confirmed	moderate	Nil
7	39	Osteo-arthritis	2–3 Year	Both Knee	85	Neg	Moderate	Not confirmed	moderate	Moderate
8	40	Osteo-Arthritis	1 Year	Right Knee	61	Neg	Mild	Not confirmed	moderate	Moderate
9	58	Reactive Arthritis	1 Year	Left Knee	22	2	Severe	Not confirmed	Moderate	Moderate
10	60	Osteo-Arthritis	4 Months	Both Knee	10	Neg	Severe	Not confirmed	Moderate	Mild
11	64	Osteo-Arthritis	15 Days	Right Knee	50	Neg	Moderate	Not confirmed	Moderate	Nil
12	72	Osteo-Arthritis	1 Year	Left Knee	34	Neg	Mild	Not confirmed	Moderate	Nil
13	81	Reactive Arthritis	4 Days	Left Knee	13	4.5	Mild	Not confirmed	Moderate	Moderate
14	84	Reactive Arthritis	1 Months	Left Knee	– 16	0.49	Mild	Not confirmed	Moderate	Nil
15	86	Reactive Arthritis	1 Month	Left Knee	10	2.00	Severe	Inflammation found	Moderate	Moderate
16	88	Reactive Arthritis	1 Year	Right Knee	50	Neg	Moderate	Not confirmed	Moderate	Nil
17	103	Not diagnosed	20 Days	Right Knee	10	6.9	Moderate	Not confirmed	Moderate	Severe
18	107	Not diagnosed	2 Years	Both Knee	15-	Neg	Severe	Not confirmed	Moderate	Moderate

information about inflammation, analysis of this hotspot helps in automatic diagnosis of diseases, making an individual treatment plan and also offers an insight into the prognosis [17]. Accurate segmentation of hotspot/inflamed region is required for further analysis. The precise segmentation of hotspot in terms of accuracy and analysis of it can have different applications:

- 1) Non-invasively early subclinical condition prediction/confirmation:** Inflammation of joint is considered as an early sign of arthritis. Hotspot detection and segmentation will help to the early detection of the subclinical condition.
- 2) Dosimetric quantification:** Inflammation describes the diseases activity in arthritis. A measure of the spread of the hotspot will specify the intensity of inflammation subjectively. The severity of inflammation provides knowledge about the diseases activity during medication. This information helps clinicians to determine dosimetric quantification during follow up [11,12].
- 3) Observer independent:** Automatic segmentation can reduce the observer intervention in the detection of the area of the hotspot.

Table 1 tabulates some cases of subclinical inflammation present in the dataset in detail. Correlation between pathological and clinical tests of patients (suffering from inflammation) with the features of the resultant hotspot is evaluated. The results will show the efficiency of the thermal image as well as hotspot segmentation in the diagnosis of subclinical inflammation. It will also pave the path for the other application of thermal image in the field of arthritis.

Segmenting the hotspot regions from the thermal images is a very challenging problem due to the presence of noise and blurry edges. The segmentation of thermal images must overcome these challenges: (1) under and over-segmentation of the hotspot leading to the inaccurate diagnosis of diseases regarding the spread of inflammation, (2) missed segmentation due to the presence of disconnected sub-regions of the hotspot [18]. The hotspot of thermal image is the Region of Interest (ROI) for the segmentation. Limited reporting of the over, under and missed segmentation of ROI in thermal images are available in the relevant literature. Several segmentation techniques exist for hotspot segmentation in thermal medical images such as FCM [20,23,24], K-Means [20–23], and Otsu's thresholding [19] based segmentation techniques were popularly employed. Furthermore, region growing is found to be very efficient in thermal image segmentation because of the natural choice of pixels with the highest intensity as initial seed points and is also found stable to noise [10]. Two Region growing is performed parallelly on two matrices for obtaining the correct segmentation. The significant contributions and advantages of this article are summarized

as follows:

- (1) Our proposed technique offers an effective hotspot/inflamed region segmentation mechanism of the ROI devoid of the associated problems of over, under and/or missed segmentation.
- (2) We introduce an automatic multi-seed point selection criterion for seed point initialization. That solves the missed segmentation problem arises due to the presence of disconnected regions in the hotspot.
- (3) It experiments on our newly created inflammatory thermal knee joint dataset [17], with clinically validated ground truths for hotspot/inflamed region segmentation.
- (4) For the nonavailability of other inflammatory knee joint dataset, an online available benchmark dataset, DMR-IR, and one newly created Breast dataset DBT-TU-JU are used for validating the performance of the method.
- (5) We also showed the significance of hotspot/inflamed region for the detection of subclinical inflammation using correlation coefficient.
- (6) A comparative study is presented between the existing state-of-the-art segmentation methods used in medical thermal images and the proposed method for proper validation and inference.

The rest of the paper is organized as the following: Section II describes the problem definition; Section III describes the proposed segmentation technique. In Section IV, we compare and analyze the outcomes of the proposed segmentation with the state-of-the-art methods. Finally, we conclude in section

2. Problem Definition

Primarily due to the inadequate specification of over, under and missed segmentation in respect of hotspot region identification in thermal images; relevant prior reporting are limited in literature as of now. Based on a small difference of temperature, thermal imaging is able to reflect abnormality in medical thermograms. Therefore, accounting small infirmations is also important for accurate analysis of the thermograms. When analysis of the ROI (Hotspot) is employed for better understanding then accurate ROI segmentation should be the first step to concern. Because improper segmentation can provide misinformation. Regarding medical importance, misinformation may lead inaccurate treatment. Given the paramount medical importance of accurate segmentation of hotspots/ROIs in thermal images for ensuring accurate diagnosis, we intend to overcome this in the present scope.

According to the metrics defined by Hoover et al. in [25], over-segmentation is identified as the multiple detections of a single region

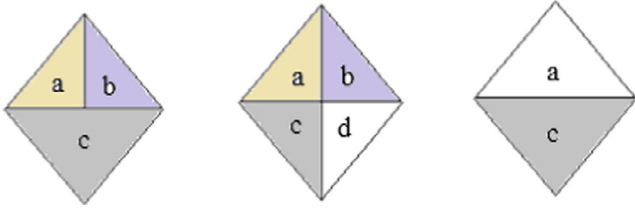


Fig. 1. (a) Ground truth Segemntation map. (b) over segmentation of the region ‘c’ that create a new segmentation ‘d’. (c) Under segmentation of region ‘a’.

results. Under-segmentation is defined as the insufficient division of multiple areas which produces a subset of the ground truth topology. Fig. 1 represented the over and under segmentation, where Fig. 1(a) is the ground truth segmentation and Fig. 1(b) and (c) describe the over and under segmentation respectively. In Fig. 1(b) the segment named as (a) is oversegmented and Fig. 1(c) segment (a) is under segmented. Both the number of segment and their corresponding area can be considered for representation of over and under segmentation.

In our case, there are only two regions in both the machine segmented image and ground truth image. One is the hotspot region (foreground), and the remaining region is considered as the background. So, the number of segments will act as a constant here and the value is 2. With respect to the hotspot, oversegmentation occur when pixels belong to the hotspot are considered as the background pixel. Undersegmentation occurs when pixels of background are considered as the foreground pixel. Fig. 2(a) shows a case of over-segmentation, Fig. 2(b) shows a case of under-segmentation, Fig. 2(c) shows a case of both under and over-segmentation in the machine segmented region whereas, Fig. 2(d) shows a case of missed segmentation since a disconnected region belonging to the ROI remains undetected [25]. Here, we are not considering the background pixels. Effect of over and under segmentation on hotspot area and background is opposite. Over-segmented hotspot area causes under segmentation of background and vice versa.

Our primary interest lies in the accurate detection of the foreground. Moreover, the accuracy of the detected hotspot is also crucial for the sake of pathological decisions. Therefore, we defined the below metrics specifically for quantify the accuracy of hotspot segmentation, based on the area of the regions, i.e., the number of pixels.

We consider the following sets: a set R_i^S consisting of all the segmented pixels in the i^{th} single disconnected sub-region of the complete ROI produced by a segmentation technique, a set R_i^G comprising all the pixels of the i^{th} single disconnected sub-region of the complete ground truth segment. Let C_R be the number of disconnected sub-regions in the segmented image and C_G be the number of disconnected sub-regions in

the ground truth image. We define:

- (1) *Over-segmentation*: A segmentation is considered as over-segmentation if $R_i^S \subset R_i^G$ for any $i, i \in C$; where, $C = C_R = C_G$.
- (2) *Under-segmentation*: A segmentation suffers from under-segmentation if $R_i^S \supset R_i^G$ for any $i, i \in C$; where, $C = C_R = C_G$.
- (3) *Over and Under-Segmentation*: There could exist both over and under-segmentation in a segmented region if,

$$R_i^S \cup R_i^G \supset R_i^S \text{ and } R_i^S \cup R_i^G \supset R_i^G$$

for any $i, i \in C$; where, $C = C_R = C_G$.

- (4) *Missed segmentation*: We identify a missed-segmentation if the condition $C_R < C_G$ satisfies.

Based on these defined metrics on thermal images, Fig. 2(e) shows an example of accurately segmented ground truth. Whereas Fig. 2(f), (g) and (h) demonstrates over, under and missed segmentation respectively.

3. Proposed Segmentation Method

We used conventional Region Growing method with modified stopping and similarity criteria with automatic seed selection procedure for segmentation of ROI from thermal image. Segmentation of original image using region growing either suffers from over segmentation or under segmentation. Implementation of existing methods indicate under segmentation is common phenomena. Overcome this problem we do not rely only on the original image. Using other features of the image we try to compensate the problem. In this scope of the paper entropy feature is used to overcome the over and under segmentation. Region growing algorithm is applied to the original image and also to the entropy image, is generated using Eq. (2). An intersection of these two results of two region growing produces the actual result. Provided both the segmentation should produce under-segmented results. If one segmentation among the two, resulting over-segmentation will lead to the incorrect segmentation. The concept is illustrated in the Fig. 3. Fig. 3(a) describes the situation when two under-segmented results are generated, and it shows there is a high possibility to provide actual ground truth. Whereas, in other two cases over segmented result will dominate the final segmentation result. Along with the original image, other features such as image energy, image contrast, homogeneity, correlation can be used, provided that both the segmentation has to persist common area. In this scope, we use entropy feature and original image for correct segmentation.

Entropy is a feature that signifies the texture of an image. Low

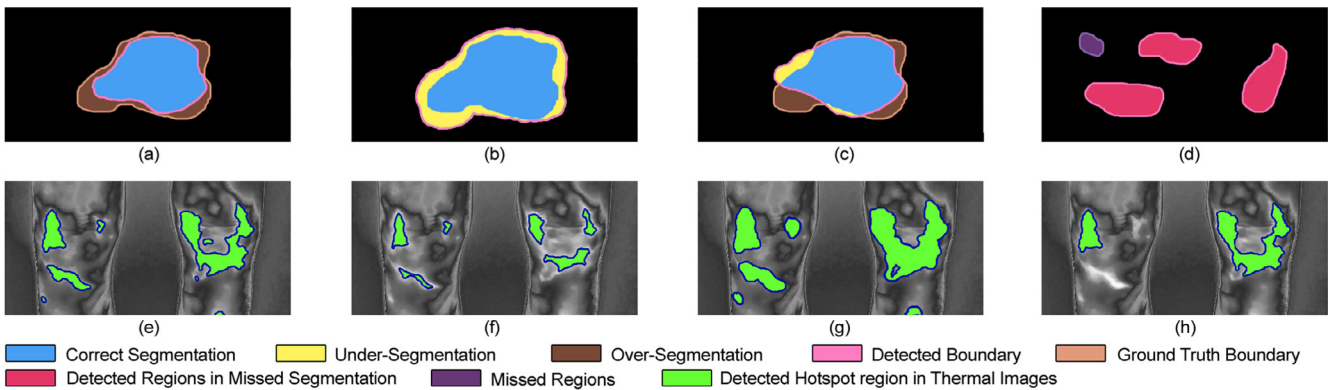


Fig. 2. (a) Over-segmentation of a single disconnected region of the hotspot, (b) Under-segmentation, the dotted line is the boundary of the region, (c) Both under and over-segmentation, the yellow region represents under-segmentation whereas the brown region represents over segmentation of the region, (d) Missed Segmentation of the hotspot region, the violet region is undetected part of the hotspot, (e) An example of correct segmentation (ground truth) of the hotspot in a thermal image (f) Over-segmentation of the hotspot in the same thermal image. (g) Under-segmentation of the hotspot (h) Missed segmentation.

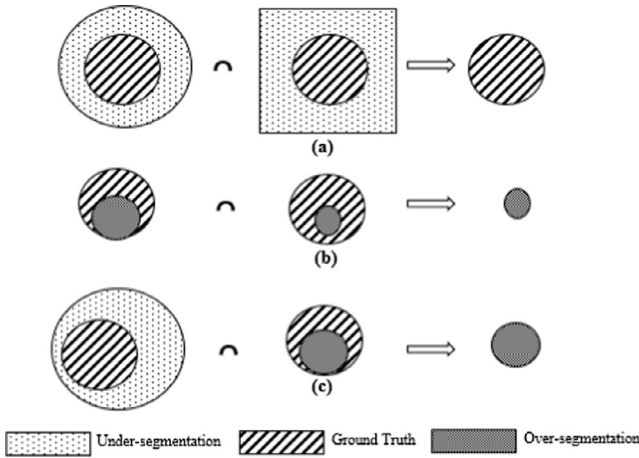


Fig. 3. (a) Intersection of two under-segmented images. (b) Intersection of two over-segmented images. (c) Intersection of one under-segmented image and one over-segmented image.

entropy defines low variation, low disorder. Therefore, Entropy feature able to signify the grouping of homogeneous pixels in order to segment thermal images.

3.1. Pre-processing

Thermal images are captured in the gray palate. Gray palate is a representation of gray images consists of three channels (24 bit). The entire three channels contain the same value i.e., the gray value. So, thermal images are converted into gray images (8 bit) that deduct two similar channels. Raw thermal images are consist of a color bar, company logo, maximum and minimum temperature points, etc. So, cropping becomes essential for further processing. We cropped thermal images manually, and gray converted images are used for later processing. Thermal images persist different kinds of noise like other imaging technology. In [36] authors presented a brief overview of noises of thermal images. They describe that images captured by LWIR camera with FPA (Focal Plane Array) persist fewer noises in indoor condition. There is more chance of noise due to emissivity fluctuation. They addressed the problem and described that if there is a large difference in the emissivity of background and the object, then it will produce negligible noise. Detector noise is also an issue in the thermal image. We used existing density estimation based noise removal [36] method for our work. As density estimation is a well known method so, we are not discussing the algorithmic steps of density estimation method.

3.2. Entropy image

Image entropy is derived from Shannon's Entropy, known as Information Entropy. Whereas, statistical entropy is used in every aspect and it is based on Boltzmann constant. Statistical entropy measures the disorder of systems as follows.

$$E = k \log T \quad (1)$$

Where E is the calculated entropy of any system, k is the Boltzmann's constant and T is the possible arrangement of microstates. Regarding image segmentation in this proposed work, image matrix is considered as a system, and pixel values are states of that system. The information of disorder plays an important role in image segmentation. So, for a given matrix T of size $M \times N$, we can derive the entropy matrix, Θ of same size i.e. $M \times N$, using following equation.

$$\Theta_{u,v} = k \log T_{u,v} \quad (2)$$

Where, u varies from 0 to $M-1$ and v varies from 0 to $N-1$. To compute

entropy for a given image, $T_{u,v}$ is computed using the Eq. (3) and Boltzmann Constant (k) is defined as the value of the maximum state, i.e. 255 which is the maximum gray level and named as 'Image Constant' specifically for the proposed method.

$$T_{u,v} = I_{u,v} + \sum_{a=-k}^{+k} \sum_{b=-l}^{+l} \left(\frac{|I_{u,v} - I_{u+a,v+b}|}{(2k+1)(2l+1) - 1} \right) \quad (3)$$

where $T_{u,v}$ is the updated pixel value calculated based on the influence of its neighbourhoods, $I_{u,v}$ is the pixel value of (u,v) coordinates. The possible arrangement of pixels with respect to the centre pixel is computed in a neighborhood of size $(2k+1)(2l+1)$. The values in Θ are then normalized within the range (0, 255) and called as an Entropy image. As discussed earlier, we individually perform region growing in both the images using their respective thresholds to obtain two separate regions, which are then intersected to get the final output. This output is considered to be more accurate reducing under-segmentation, rationalized in the next sub-section.

3.3. Modified Region growing algorithm

The Conventional Multi-seeded Region Growing technique (CMRG) requires single/multiple seed points and a threshold to start the segmentation [27]. By assimilating homogeneous neighbor pixels, the segment grows iteratively. The resulting segmentation could highly depend on the initial seed chosen, the threshold value and the criteria in which neighboring pixels are examined. The selection of homogeneity criteria in region growing relies not only on the problem under consideration but also on the type of image subjected to segmentation. There are three major issues in the CMRG [27]. They are (1) Selection of seed points, (2) Similarity and connectivity criteria, (3) Termination of the segmentation process (Stopping rule).

Properties of the thermal image ensure the effectiveness of region growing in hotspot segmentation. Hotspot area of the thermal image comprises the highest pixel values. So, it makes the seed selection procedure easier. Highest pixels of the thermal image are considered as seed during thermal image segmentation. The boundary of the region is detected by the stopping criteria. Stopping criteria should be well defined, that it can identify actual region boundary. Stopping criteria is dependent on the image features. Pixel intensity threshold values, image histogram, etc. are often used as the stopping criteria. Hence, justifiably we use the pixels with the highest intensity value as the seed points in every epoch. Considering the seed point with the coordinate (u, v) , we define two variables α and β , which are initialized to $I_{u,v}$ and $\Theta_{u,v}$ respectively. Each pixel in the 8-neighborhood (N_8) of the seed point is considered for comparison using Eq. (4), providing thereby the similarity criteria and stopping rule. Initially $\xi = \phi$, $\omega = \phi$ and ξ, ω are the resultant region from the two input matrix I and Θ .

$$\begin{aligned} \xi &= \xi \cup \{(x, y) \mid |\alpha - I_{x,y}| < \rho\} \\ \omega &= \omega \cup \{(x, y) \mid |\beta - \Theta_{x,y}| < \tau\} \end{aligned} \quad \left| \begin{array}{l} I_{x,y}, \Theta_{x,y} \in N_8 \text{ of } I_{u,v} \end{array} \right. \quad (4)$$

where, two variables α and β , are updated using Eq. (5) when new pixels from the neighborhood of any boundary pixel is/are identified in the "detected region,".

$$\begin{aligned} \alpha &= \frac{1}{n_1} \sum_i^{n_1} p_{x_i, y_i} \quad \text{where, } (x, y) \in \xi \text{ and } n_1 = |\xi| \\ \beta &= \frac{1}{n_2} \sum_i^{n_2} q_{x_i, y_i} \quad \text{where, } (x, y) \in \omega \text{ and } n_2 = |\omega| \end{aligned} \quad (5)$$

where, p represents the pixel value from image I with the position (x,y) and q represent the pixel value from image Θ with the position (x,y) . We used trial and error method for selection of a threshold for stopping criteria, detailed in section IV-E. The conditions in Eq. (4) are followed in each iteration growing the detected region while updating the variables α and β in every iteration. When the iteration stops, the final set of pixel coordinates ξ and ω are produced. The above description is based on the region growing procedure using single seed. From the

observation of dataset it is evident that disconnected hotspot regions are present in thermal images. If more than one regions exist than single seed based region growing will fail in detecting all the disconnected regions. So, Proposed method uses region growing algorithm which is based on multiple seeds. The procedure for selecting multiple seeds discussed in section III-D. Multi seed based region growing algorithm is an extension of single seed based region growing. For multiple seeds there may be multiple segments.

Let us consider for image I and Θ , region growing algorithm has found out m_1 and m_2 segments respectively. ξ_i is the detected intermediate ROI grown from the i^{th} seed point. The same process is repeated for all the remaining seed points only if they do not belong to the already detected hotspot region ξ_i .

$$\Xi = \Xi \cup \xi_i \quad (6)$$

where i varies from 0 to m_1 . The final region output Ξ is computed using Eq. (6) which is the union of ξ_i 's detected from all the m_1 seed points. In the same way the Ω is calculated from the obtained ω_i , where i varies from 0 to m_2 , given in Eq. (7).

$$\Omega = \Omega \cup \omega_i \quad (7)$$

To appreciate the significance of Eq. (4) in tackling under and over segmentation, we assume the formation of two different sets of pixel coordinates during the process of region growing. These two sets are denoted as Ξ and Ω .

from the above discussions and equations it is clear that Ξ and Ω are two output obtained from the two image I and Θ . They are equal in size, they consist of the same background. But for multi seed region growing that may consist a different number of segments. So, the intersection of between them will deduct the small and inessential segments.

Provided, both Ξ and Ω are inaccurate due to under-segmentation, their intersection could be perceived as less under-segmentation, proved in Theorem 1. The proposed method gives the final segmented region Φ_{roi} as the intersection of Ξ and Ω , given in Eq. (8).

$$\Phi_{roi} = \Xi \cap \Omega \quad (8)$$

Since the intersection of two independent sets of pixels is outputted as the final segmented ROI (Φ_{roi}), the under-segmentation problem of CMRG may be avoided specifically. To prove this, let us consider the following sets: a set R_s consisting of all the segmented pixels of a single disconnected sub-region produced by the CMRG. Set G_s consisting of all the pixels of a single disconnected sub-region of the corresponding ground truth segment. We assume three cases of CMRG segmentation. The cases are:

Case 1:. The output of CMRG technique is under-segmented, i.e.,

$$R_s \supset G_s \quad (9)$$

Case 2:. The output of CMRG technique is over-segmented, i.e.,

$$R_s \subset G_s \quad (10)$$

Case 3:. The output of CMRG technique is both over and under-segmented, i.e.,

$$R_s \cup G_s \supset G_s \text{ and } R_s \cup G_s \supset G_s \quad (11)$$

Postulate 1: The sets ξ and ω , both individually follow these three cases of R_s since their formation is similar to the CMRG technique.

Theorem 1:. The segmented pixels set Φ_{roi} is a proper subset of the pixel set R_s when R_s is under-segmented, i.e. case 1.

Proof: Based on Eq. (9), i.e. $R_s \supset G_s$ and Postulate 1, the sets ξ and ω follow Eq. (12).

$$\xi \supset G_s \text{ and } \omega \supset G_s \quad (12)$$

Substructing, the relations of ξ and ω in Eq. (12), we get,

$$\xi - \omega \supset G_s - G_s \text{ when, } \xi \supset \omega \quad (13)$$

Or

$$\omega - \xi \supset G_s - G_s \text{ when, } \omega \supset \xi \quad (14)$$

Since, $G_s - G_s$ is a null set ϕ , Eq. (13) and Eq. (14) can be written as,

$$\xi - \omega \supset \phi \text{ when, } \xi \supset \omega \quad (15)$$

Or

$$\omega - \xi \supset \phi \text{ when, } \omega \supset \xi \quad (16)$$

From Eq. (15) and Eq. (16), we can imply the below relationship,

$$(\xi - \omega) \cup (\omega - \xi) \supset \phi \quad (17)$$

Now the symmetric difference in Eq. (17) can be written as,

$$(\xi \cup \omega) - (\xi \cap \omega) \supset \phi \quad (18)$$

Combining Eq. (8) with Eq. (18), we get the below relationship,

$$(\xi \cup \omega) - \Phi_{roi} \supset \phi \quad (19)$$

Since the difference between the union of the two sets ξ and ω and Φ_{roi} is greater than ϕ . So, we can say that the output set Φ_{roi} contains at least 1 pixel less than the output set of CMRG, R_s . Therefore, from Eq. (19) it could be concluded that $\Phi_{roi} \subset R_s$. This implies the occurrence of less under-segmentation in Proposed method compared to the CMRG. However, if case 1 is true, then over-segmentation may take place.

Theorem 2:. The ground truth set G_s is a proper subset of the segmented pixel set Φ_{roi} when R_s is under-segmented, i.e. case 1.

Proof: Intersecting, the relations of ξ and ω in Eq. (9), we get the below relationship,

$$\xi \cap \omega \supset G_s \cap G_s \quad (20)$$

This can be written as,

$$\xi \cap \omega \supset G_s \quad (21)$$

Hence from Eq. (8) and Eq. (21),

$$\Phi_{roi} \supset G_s \quad (22)$$

From Eq. (22), we can imply that the set Φ_{roi} is a smaller set than the ground truth segment set G_s . This proves the absence of over-segmentation in proposed segmentation process. However, in such a case under-segmentation cannot be totally ignored.

Theorem 3:. The segmented pixel set Φ_{roi} is a proper subset of ground truth set G_s when R_s is over-segmented, i.e. case 2.

Proof: Based on Eq. (10), i.e. $R_s \subset G_s$, we can assume that the sets ξ and ω follow Eq. (23) since their formation is similar to the CMRG.

$$\xi \subset G_s \text{ and } \omega \subset G_s \quad (23)$$

Intersecting, the relations of ξ and ω in Eq. (23), we get the below relationship,

$$\xi \cap \omega \subset G_s \cap G_s \quad (24)$$

This can be written as,

$$\xi \cap \omega \subset G_s \quad (25)$$

Hence from Eq. (8) and Eq. (25),

$$\Phi_{roi} \subset G_s \quad (26)$$

From Eq. (26), we can imply that the set Φ_{roi} is a smaller set than the ground truth segment set G_s . This proves the absence of under-segmentation in proposed segmentation process.

Theorem 4:. The segmented pixel set Φ_{roi} is a proper subset of ground truth set G_s when only any one of the ξ and ω is over-segmented, i.e. case 1 and 2 both occur.

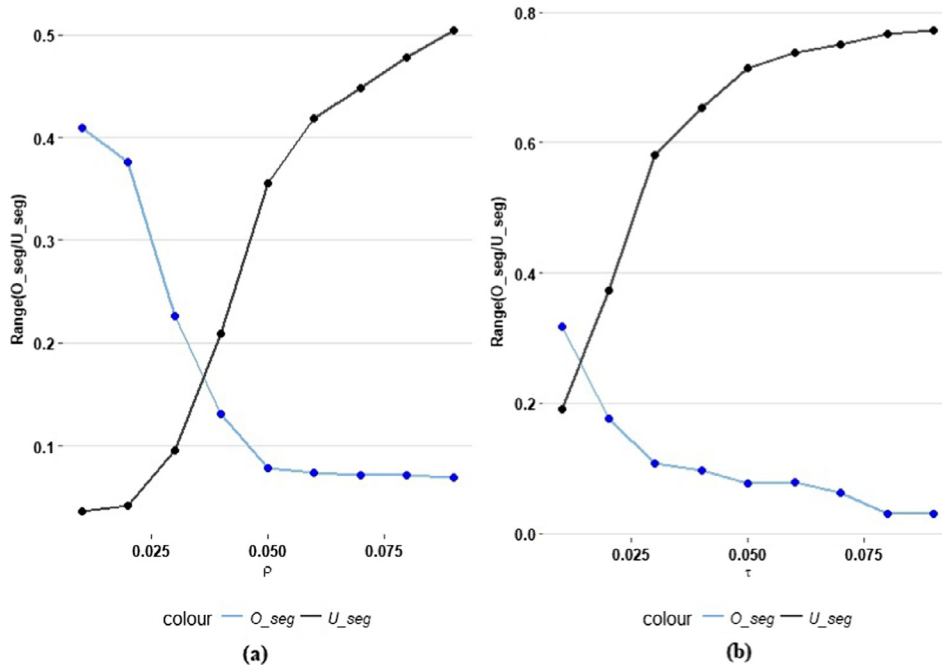


Fig. 4. Graphical comparison of the effects of thresholds with respect to U_{seg} and O_{seg} measures in both the data sets: (a) Energy threshold in knee data set, (b) Entropy threshold in knee data set.

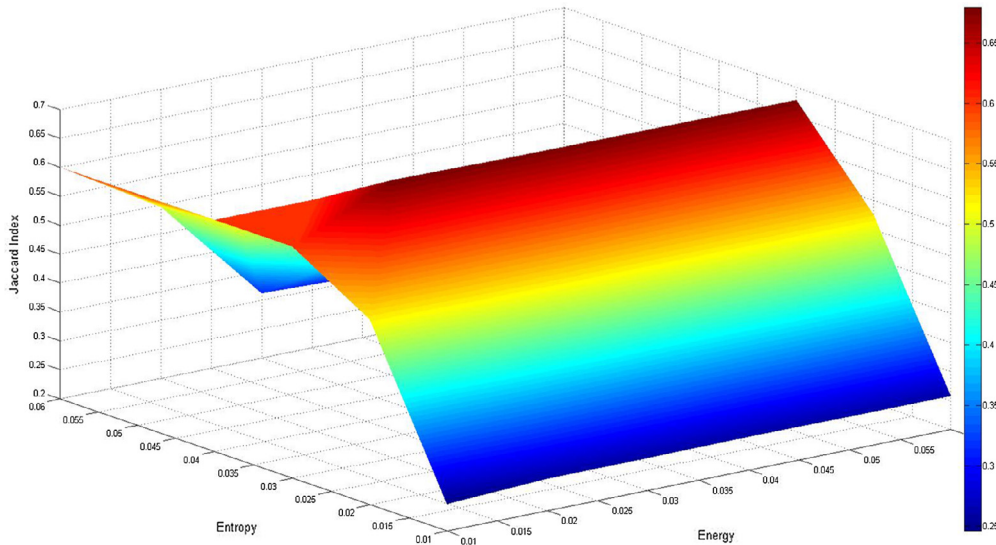


Fig. 5. Plot the effects in segmentation Jaccard Index with respect to both thresholds for knee data set.

Proof: When case 1 and 2 both occur, i.e., if ξ is over-segmented while and ω is under-segmented or vice versa, assuming ξ as the over-segmented set and ω as the under-segmented set we can write the following,

$$\xi \subset G_s \text{ and } \omega \supset G_s \tag{27}$$

From Eq. (27), we can infer,

$$\xi \subset G_s \subset \omega \tag{28}$$

Now, Eq. (28) can be written as,

$$\xi \subset \omega \tag{29}$$

Based on Eq. (29), we can conclude that,

$$\xi \cap \omega = \xi \tag{30}$$

Combining, $\xi \subset G_s$ and Eq. (30) we can write,

$$\xi \cap \omega \subset G_s \tag{31}$$

Hence from Eq. (8) and Eq. (31), we get,

$$\Phi_{roi} \subset G_s \tag{32}$$

From Eq. (32), we can imply that the set Φ_{roi} is a smaller set than the ground truth segment set G_s . This proves the absence of under-segmentation in such a case. The same could be proved when ξ as the under-segmented set and ω as the over-segmented set.

If anyone of ξ and ω is over-segmented or both of them are over-segmented, then over-segmentation cannot be avoided. Hence, to avoid over-segmentation, we choose the thresholds ρ and τ accordingly. Furthermore, if case 3 occurs, the proposed method unable in reducing both under and over-segmentation. Although, since Φ_{roi} could be a smaller set than ξ and ω , either of the following results may occur: 1) Φ_{roi} causes more over-segmentation than ξ and ω , 2) Φ_{roi} causes less

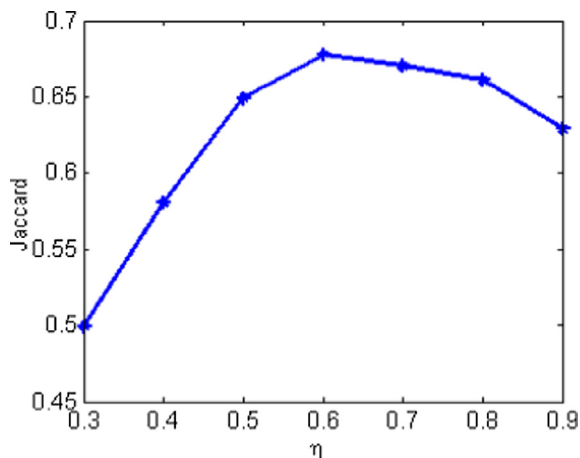


Fig. 6. The effect in Jaccard Index (JI) with respect to the parameter (η).

under-segmentation than ξ and ω , 3) Φ_{roi} together causes more over-segmentation as well as less under-segmentation than ξ and ω .

3.4. Automatic selection of seed points

Missed segmentation should be handled by any segmentation method for correct segmentation. Thermal images may contain disconnected hotspot regions, with the pixel values of different ranges. Since in thermal images, CMRG technique assumes the pixels with highest gray value as seed points, the hotspot regions having pixels smaller than the highest gray value are bound to remain undetected. In that event, there is a high probability of missed segmentation. To solve this issue, we introduce criteria for seed point selection. The pixels with the highest gray value are selected as the initial seed points for the first epoch. After the i^{th} epoch, seed points are again selected for the next epoch using two criteria. Firstly, the seed points are the pixels with the highest gray value among all the pixels of the input image excluding the ones already included in the first epoch, i.e. the current Φ_{roi} . Secondly, the highest pixel (say P) must satisfy Eq. (33),

$$P > \min(\Phi_{roi}) + [\eta \times \{\max(\Phi_{roi}) - \min(\Phi_{roi})\}] \quad (33)$$

where $\min(\Phi_{roi})$ is the minimum gray value in Φ_{roi} , $\max(\Phi_{roi})$ is the maximum gray value in Φ_{roi} . And η is a real number whose value can lie in the range [0,1]. The value of η can vary for different datasets. We obtained the best results using $\eta = 0.74$ for both data sets (see section IV-D). At the beginning of each epoch, new seed points are calculated. A pixel is considered as a seed point for the next epoch only if its gray value exceeds a certain integer (say k). Let us assume the intermediate segmented set of pixels Φ_{roi} in the j^{th} epoch has the lowest gray value (say a) and the highest gray value (say b). Therefore in the $(j + 1)^{th}$ epoch k must lie in between a and b where, $k = a + \eta(b - a)$. This indicates the gray value of the seed point must be greater than k . We assume each disconnected hotspot region in the ROI must contain at least one pixel with a gray value greater than k . Hence, the missed segmentation can be reduced using Eq. (33) but may not be eliminated.

3.5. Thermal imaging in the detection of inflammation:

This literature primary focus is the detection of subclinical inflammation through Thermal Images. The literature aims to prove the efficacy of Thermal Images in detection of subclinical inflammation through proving its efficacy in accurate detection of inflammation. ROI extraction is the first step of the analysis. Association between ROI features and clinical test data is a way to describe the relationship between them. The correlation between features of ROI extracted from the thermal image, and the ESR or CRP for the known cases are evaluated. Positive correlation will prove that the thermal image can detect the

inflammation. Hence, thermal image able to provide a decision regarding subclinical inflammation for better disease prognosis. The correlation coefficient is employed here for this purpose. The correlation coefficient is a well known and simple method, often used for data analysis. Correlation coefficient represents the degree of association between two linearly related datasets. A linear relationship should exist between datasets to find the correlation. Scatter plot and trend line on the scatter plot is evidence of a linear relationship between the given dataset. The scatter plot, trend line and resultant correlation between the features of ROI from thermal images and pathological tests is shown in Fig. 10.

4. Experimental results & discussions

4.1. Database preparation

The proposed segmentation technique in our work was tested on three thermal medical image datasets: (1) DBT-TU-JU breast dataset [15] (40 images), (2) DMR-IR breast dataset [16], designed by Silva et al. (44 images), and (3) a new inflammatory knee joint dataset [17] (50 images), which was created and collected from the Physical Medicine and Rehabilitation (PMR) Department, Agartala Government Medical College (AGMC) and Regional Cancer Center (RCC), Govind Ballav Pant Hospital (GBP), Agartala, Tripura, India. The first and second dataset contains Breast images with an abnormality such as ductal breast cancer, malignant, and benign tumor, etc. The third dataset consists of thermal images of different inflammatory pain-related diseases of knee joints such as Osteo Arthritis, Rheumatoid Arthritis, Reactive Arthritis, Mono Arthritis, etc.

4.2. Clinical validation of the datasets

Medical data analysis consist an important phase which is validation. Validation referred to the comparison of acquired data with medical data. Medical data are profusely used for disease confirmation for more than several years. So, diseases confirmation of acquired data should be validated using medical history. Hence, it is considered an important part of medical image processing. DBT-TU-JU and DMR-IR datasets were already validated clinically in [15] and [16], respectively. The newly created inflammatory knee joint dataset of 50 thermal images was validated by examining the Arthritis patients. Presence of inflammation is validated using ESR or CRP by physicians. We also used these two blood markers for validation purpose. Clinical examination by a physician is also incorporated here for validation. ESR, CRP and clinical examination result found positive for maximum numbers of inflammatory arthritis data, and negative for non-inflammatory data. Among these three factors if three of them are found positive than physician consider it as positive and vice-versa for negative cases. We consider these three factors in validating our data. The positive and negative cases are considered in this work follow these validation process. Subclinical inflammation in arthritis joint is considered when physician unable to assess the inflammation condition. ESR and CRP also found unable to help physician. We consider these cases and a physician also confirmed the subclinical conditions.

4.3. Generation of ground truth

Ground truth creation for all the three datasets was necessary to verify the competence of the proposed technique in comparison to the state-of-the-art. An alternative solution is the creation of ground truths using manual segmentation [28]. Manual segmentation is considered as the most reliable method for segmentation to identify the shape and the structure of a particular clinical task. A doctor/clinician has more knowledge and idea about the diseases, its spread, and its origin. Only they can recognize the affected area appropriately, and for that, ground truths should be validated by the expert doctors. Ground truths for the

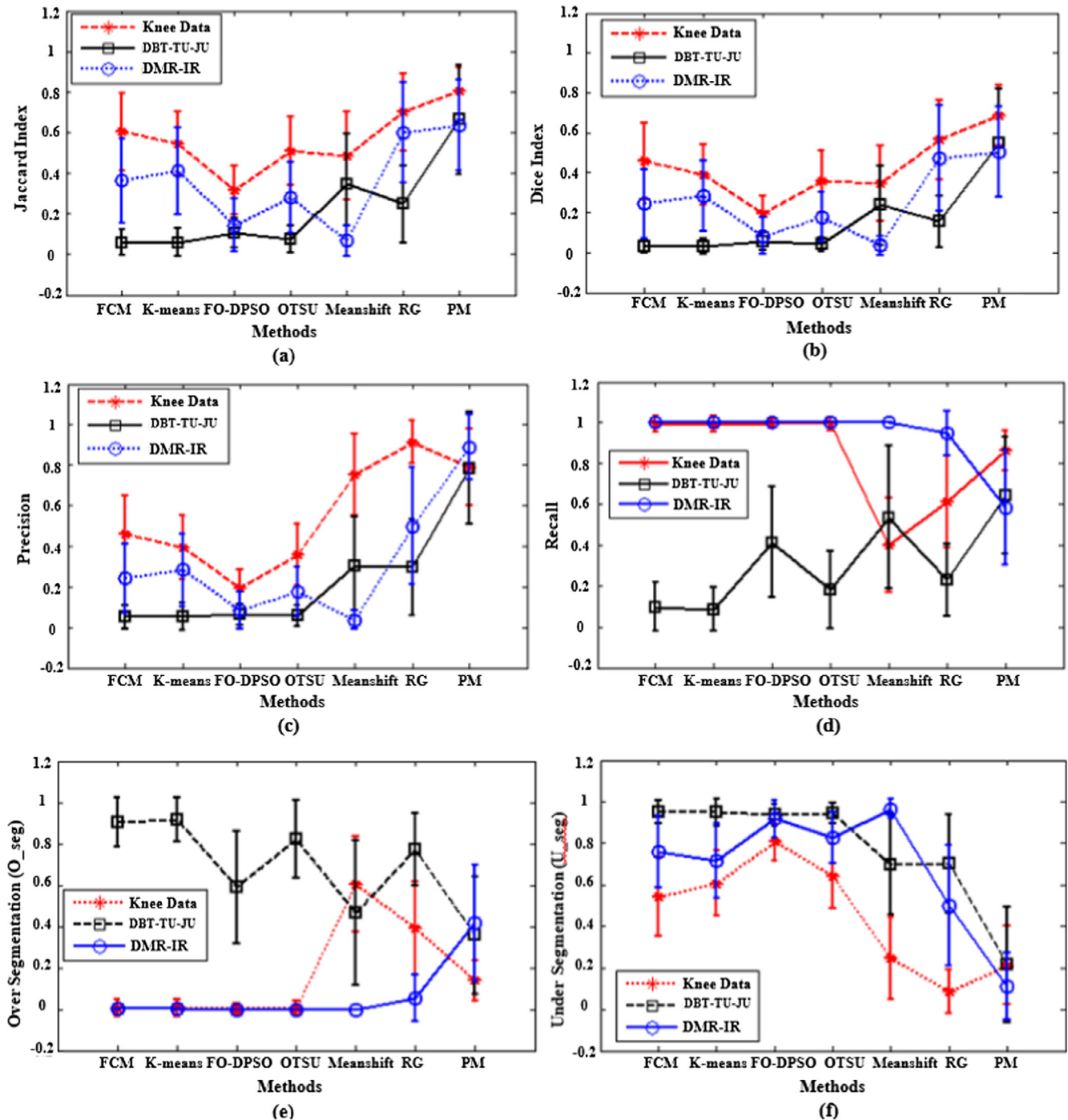


Fig. 7. Jaccard Index, Dice Index, Precision, Recall, Over segmentation and under segmentation rate for all dataset used. Here, the Knee Data referred to the the newly designed inflammatory knee joint dataset All values are given as mean \pm standard deviation vs. each method. (b) and (c) are considered together for representing accuracy, there should be little difference between the precision and recall for each method. (e) and (f) are also considered together, over and under segmentation both should be near to '0' for obtaining accurate segmentation.

datasets were created in two consecutive steps. Firstly, seven thermal image experts/technicians independently traverse the hotspot region of the thermal images to generate ground truth images using the GNU Image Manipulation Program (GIMP) [29] software. In the next step, pixel wise voting policy is considered to find the final output ground truth image. In pixel-wise voting policy, if a pixel is regarded as a foreground pixel by maximum of four technicians, then it is counted as a foreground pixel. By classifying each pixel based on this method a final ground truth is generated. In the second step, the medical expert (doctor) analyze final ground truth and finalize them.

4.4. Performance measures

Different quantitative measures have been used to analyze the performance of proposed segmentation with the state-of-the-art with the clinically validated ground truth. Theoretically proven in the previous section that proposed method reduces both under and over-segmentation concerning the RG technique. Articulating our primary focus, we quantify over and under-segmentation using (O_{seg}) and (U_{seg}) measure respectively described in [26]. O_{seg} quantifies the amount of over-segmentation in the resultant segmented image concerning its

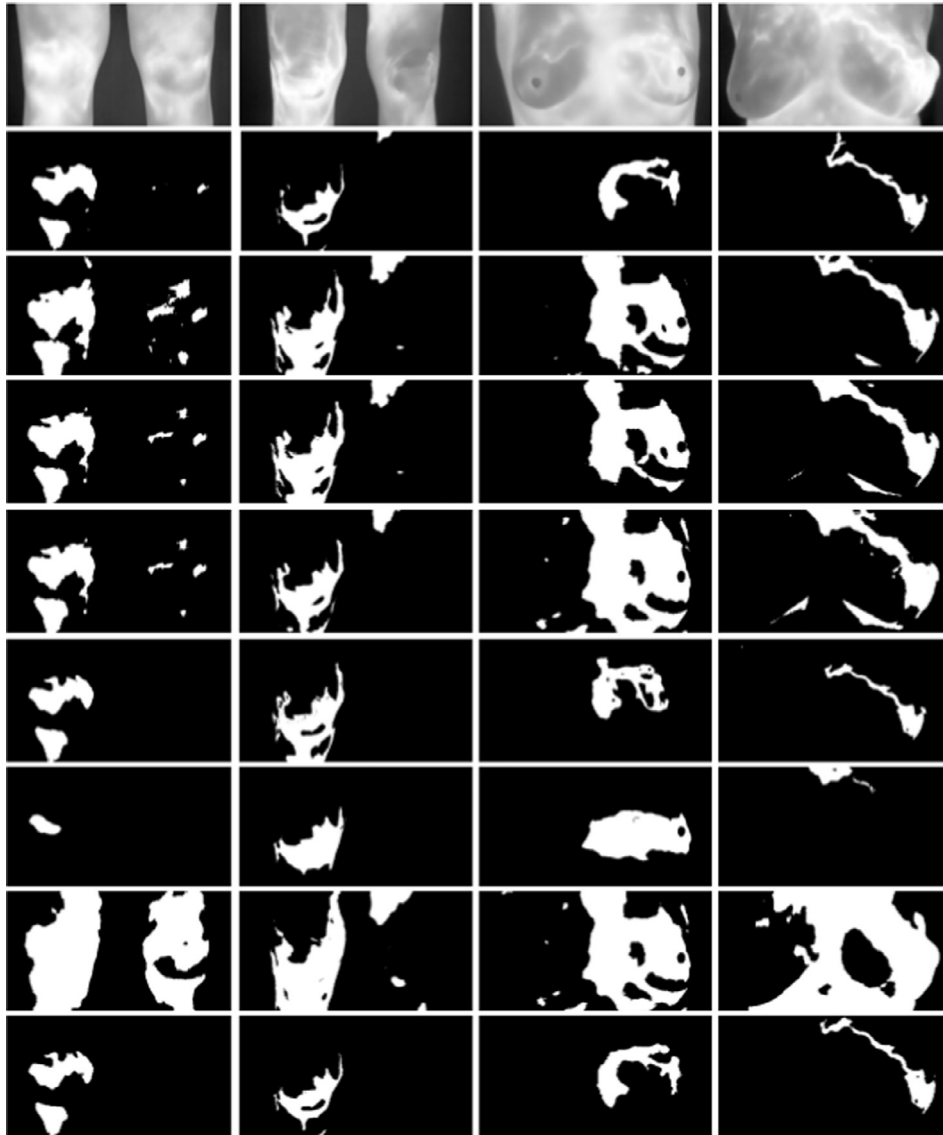


Fig. 8. Comparison of ROI segmentation in knee and breast data set. Row 1: Original Image, Row 2: Ground Truths, Row 3: Result of K-Means, Row 4: Result of FCM, Row 5: Otsu's Thresholding, Row 6: Region Growing (RG), Row 7: Mean Shift, Row 8: FO-DPSO segmentation, Row 9: Proposed Segmentation Method.

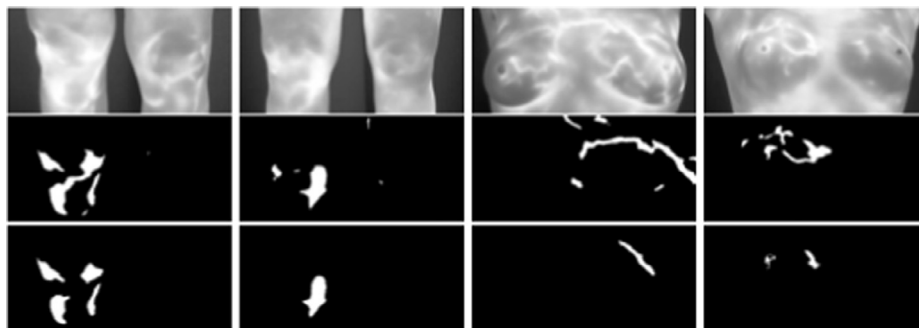


Fig. 9. Failure cases. Row 1: Original images. Row 2: Corresponding Ground truths. Row 3: Output of Proposed method.

ground truth. If the value of O_{seg} is 0 (zero) for any segmented image, it refers to no over-segmentation. Similarly, to what extent a segmentation method resist under-segmentation is quantified by the U_{seg} measure. Apart from these two measures the following measures are also used: (1) Jaccard index (JI) [30,31,34] (2) Dice similarity index (DS) [30], (3) Recall (RC) [30], (4) Precision (PRC) [30,35]. The Jaccard Similarity Index (JI) is an accepted measure for evaluating the

efficiency of any segmentation method. JI works well for larger and simple shaped objects [32]. JI measures the similarity between ground truth and segmented image and varies between (0,1), where, 1 (one) indicates a perfect overlap of the compared segmentation. DS index quantifies the overlapping of the ground truth and segmented image. The value of DS also varies between the range of (0,1) where 1 indicates good segmentation. Recall (RC) & Precision (PRC) are popularly used

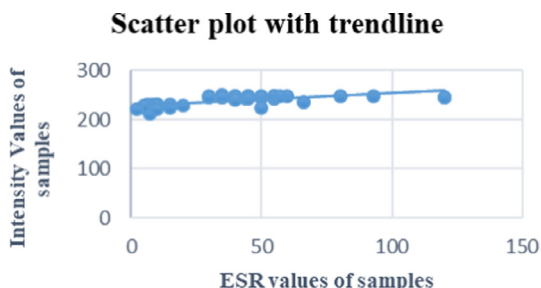


Fig. 10. Comparison of ROI segmentation in knee and breast data set.

together to identify the effectiveness of a segmentation technique. Higher the value of RC and PRC, better the performance of the technique. Among these two measures, if the value of one is higher than the other with a significant difference, that implies less accuracy.

4.5. Thresholds and parameter selection

An optimal thresholds ρ and τ were selected separately for both the datasets to test our technique. Both ρ and τ vary in the range of (0,1). The thresholds are chosen such that we achieve a little under-segmentation intentionally. To find the optimal thresholds for all the datasets separately, we have studied the plot pattern between a series of thresholds with both U_{seg} and O_{seg} measures. Plot pattern of thresholds for knee dataset have shown in Fig. 4(a) & (b). The black dotted line represents the under-segmentation effects for a threshold whereas the blue dotted line represents the effects in the over-segmentation measure. The y-axis contains a general range of over and under-segmentation values. The plot suggests that with the increase in the threshold values under-segmentation increases, whereas over-segmentation decreases. In all the cases we obtain a threshold point (say J) where the curve of U_{seg} and O_{seg} intersects with each other. This threshold value J theoretically produces the perfect segmentation when the region is growing is done using a single threshold. Hence, we choose the threshold point slightly higher than J to produce little under-segmentation as per our necessity described in the previous section. Based on the plot results, we choose ρ as 0.03 and τ as 0.02 for the inflammatory knee joint dataset whereas choosing ρ as 0.03 and τ as 0.02 for the DMR-IR breast dataset. The plot in Fig. 5 illustrates that the best segmentation accuracy was attained using the selected thresholds for knee data set. The performance of the algorithm does show dependency on the choice of the parameter η , selected between the range of (0,1). The plot in Fig. 6 illustrates that the best segmentation was achieved with η in the range 0.6 and 0.7 for all the datasets ($\eta = 0.66$ for the DBT-TU-JU dataset, $\eta = 0.7$ for the DMR-IR dataset, and, $\eta = 0.7$ for the knee joint dataset).

5. Results and discussions

We compared the proposed technique with other recent and/or widely accepted state-of-the-art segmentation methods which were successfully used for medical thermal image segmentation. Such techniques for this purpose include: (1) Otsu's Thresholding, (2) K-means segmentation, (3) Fuzzy-C-Means (FCM), (4) Mean-shift Segmentation, and (5) Region Growing (RG) [27], and (6) FO-DPSO: Fractional Order Darwinian Particle Swarm Optimization [33]. The performance of the proposed method also validates by performing it on two baseline breast dataset discussed in section IV-A, which are available online. The dataset contains breast images with an abnormality such as ductal breast cancer, malignant, and benign tumor, etc. The comparison between the seven state-of-the-art techniques along with the proposed method is indicated in Fig. 7 regarding average over-segmentation (O_{seg}) and average under-segmentation (U_{seg}) along with the Jaccard Index, Dice Index, Recall and Precision. Also, the standard deviation is shown in a

graph with error bars. With O_{seg} and U_{seg} suggest that the proposed technique can obtain better results than the state-of-the-art in both the datasets. The results imply the proposed method can serve as an efficient alternative technique for thermal medical image segmentation. Segmentation outputs of the proposed technique along with the state-of-the-art methods are compared in Fig. 8. The datasets are not followed a normal distribution. Therefore, to find the statistical significance of the values of performance measures Kruskal-Wallis P-test is used. Kruskal-Wallis P-test is a non-parametric statistical significance measure. The result of P-test for different methods are less than 0.05 that means the accuracy of the proposed method is statically significant.

As proven in the previous section, proposed segmentation suffers relatively less from under-segmentation, compared to the RG. This behavior is explained in Theorem 1. But the over-segmentation issue is not entirely resolved. As per Theorem 2, there should not be any over-segmentation. We assume in (11) that, ξ and ω are a proper subset of G_s , and $\omega \supset G_s$. Although, (31) is true for all cases, (9) may not satisfy in few cases resulting in over-segmentation.

$$|\xi| > |G_s| \text{ and } |\omega| > |G_s| \quad (34)$$

From the experimental analysis, we have observed that segmenting the two breast datasets was more challenging than the knee joint dataset. Compared to the breast datasets, all the segmentation methods discussed in this paper including our proposed segmentation method perform better on the knee joint dataset. It also observed that all the other method are prone to produce under segmented results. This the reason why we do the intersection of the two methods. Our methods failed to segment accurately when both the RG deliver over segmented results. Some examples are shown in Fig. 9.

Fig. 10. Shows the scatter plot of ESR values and feature values obtained from the ROI. The trend line of the scatter plot shows the linearity of datasets. A line can be a plot in the scatter graph that has nearly the same distance from all the data. It is enough as evidence of linearity between the datasets. The x-axis represents the ESR or CRP values of samples, and Y-axis represents the mean intensity of segmented ROI. A linear relationship between data, as proved through the scatter plot, the correlation coefficient can be applied to the data. The correlation coefficient between infrared datasets and blood markers found +0.5. The correlation coefficient value 0.5 implies a moderate linear relationship between the datasets. That means intensity mean of ROI found high when ESR or CRP values are high. The conclusion that Thermal Images can detect inflammation as blood tests (ESR and CRP) can be drawn from the result. So, thermal imaging able to improve accuracy in diagnosing subclinical inflammation if it is used along with the other diagnosing criteria. The gain i.e achieved by using thermal imaging in detection of subclinical inflammation, able to significantly modify the way arthritis patients would be managed.

6. Conclusion

There prevails lack of algorithms that automatically segment the hotspot region from the medical thermal images of different diseases. In this paper, we have proposed a method, a new scheme to segment the hotspot region in the thermal images of inflammatory knee joints efficiently. It lends itself to an automatic approach with a manually adjusted threshold value that is simple to implement and quite generalized for other thermal medical image applications. The proposed approach substantially balances the over, under and missed-segmentation, thus providing the segmenter a tool to attain acceptable segmentation quality. We have already discussed that proposed segmentation method is an extension of the RG technique, so the expectation should be to get better results compared to that and it stood to the necessary expectations with higher scores in all the measures. It also performs competitively along with the recent state-of-the-art segmentation techniques. The proposed scheme may be used in developing health abnormality detection systems based on thermal images in future

scope.

Acknowledgment

The research work was supported by the Grant No. 5/7/1516/2016-RCH, Dated 20/06/2017 from the Indian Council of Medical Research (ICMR), Government of India. The study was approved by the Ethical committee of Agartala Government Medical College with Ethics Committee approval number Ref.No.4(6-11)-AGMC/Medical Education/Ethics Com/2018/15136, Dated 31st December, 2018.

The first author would like to thank Dr. S.B.Nath, Assistant Professor & HOD I/C, Department of Physical Medicine and Rehabilitation, Agartala Government Medical College (AGMC), Agartala and Dr. Gautam Majumder, Assistant Professor, Department of Radiotherapy, AGMC and Medical Superintendent, Regional Cancer Centre, Tripura for their kind support to carry out this work.

References

- [1] Iain B. McInnes, Georg Schett, The pathogenesis of rheumatoid arthritis, *N. Engl. J. Med.* 365 (23) (2011) 2205–2219.
- [2] “Arthritis: Causes, Signs, and Diagnosis,” Healthline. [Online]. Available: <https://www.healthline.com/health/arthritis>. [Accessed: 15-Feb-2018].
- [3] Y.-C. Chen, J.-F. Chen, T.-T. Cheng, SAT0092 prevalence of subclinical inflammation in patients with rheumatoid arthritis who have low disease activity: Table 1, *Ann. Rheum. Dis.* 75 (2) (2016).
- [4] H. Daghestani, V. Kraus, Inflammatory biomarkers in osteoarthritis, *Osteoarthritis Cartilage* 23 (11) (2015) 1890–1896.
- [5] C.H.C.A. Díaz, M.R.-S. Roman, A. Vargas, A. Lopez-Macay, M.S. Olmedo, A.L. Reyes, C. Pineda, L.V. Rios, SAT0180 subclinical Inflammation in Rheumatoid Arthritis (RA) in clinical remission, lack of association between cytokines level and ultrasound-defined synovitis, *Ann. Rheum. Dis.* 73 (Suppl 2) (2014) pp.
- [6] S. Bhasin, P.P. Cheung, The role of power doppler ultrasonography as disease activity marker in rheumatoid arthritis, *Dis. Markers* 2015 (2015) 1–9.
- [7] L. Hunt, G. Eugénio, A.J. Grainger, Magnetic resonance imaging in individuals at risk of rheumatoid arthritis, *Best Practice Res. Clin. Rheumatol.* 31 (1) (2017) 80–89.
- [8] S. Omoigui, The biochemical origin of pain: The origin of all pain is inflammation and the inflammatory response. Part 2 of 3 – Inflammatory profile of pain syndromes, *Med. Hypotheses* 69 (6) (2007) 1169–1178.
- [9] B.F. Jones, A reappraisal of the use of infrared thermal image analysis in medicine, *IEEE Trans. Med. Imaging* 17 (6) (Dec. 1998) 1019–1027.
- [10] R.C. Gonzalez, R.E. Woods, *Digital image processing*, Pearson, New York, NY, 2002.
- [11] M. Palmer, TH-E-209-00: radiation dose monitoring and protocol management, *Medi. Phys.* 43 (6) (2016) 3902–3902 Part 47.
- [12] T. Takeda, Treatment strategy of elderly rheumatoid arthritis, *Japanese J. Clin. Immunol.* 39 (6) (2016) 497–504.
- [13] U.R. Gogoi, G. Majumdar, M.K. Bhowmik, A.K. Ghosh, D. Bhattacharjee, Breast abnormality detection through statistical feature analysis using infrared thermograms, 2015 International Symposium on Advanced Computing and Communication (ISACC). (2015). <http://doi.org/10.1109/isacc.2015.7377351>.
- [14] S. Bardhan, M.K. Bhowmik, S. Nath, D. Bhattacharjee, A review on inflammatory pain detection in human body through infrared image analysis, 2015 International Symposium on Advanced Computing and Communication (ISACC). (2015). <http://doi.org/10.1109/isacc.2015.7377350>.
- [15] M.K. Bhowmik, U.R. Gogoi, G. Majumdar, D. Bhattacharjee, D. Datta, A.K. Ghosh, Designing of ground truth annotated DBT-TU-JU breast thermogram database towards early abnormality prediction, *IEEE J. Biomed. Health Inform.* (2017) 1, <https://doi.org/10.1109/JBHI.2017.2740500> L.
- [16] L.F. Silva, D.C.M. Saade, G.O. Sequeiros, A.C. Silva, A.C. Paiva, R.S. Bravo, A. Conci, A new database for breast research with infrared image, *J. Medi. Imag. Health Inform.* 4 (1) (2014) 92–100.
- [17] M.K. Bhowmik, S. Bardhan, K. Das, D. Bhattacharjee, S. Nath, Pain related inflammation analysis using infrared images, *Thermosense: Therm. Infrared Appl. XXXVIII* (2016), <https://doi.org/10.1117/12.2223425>.
- [18] P. Karasev, I. Kolesov, K. Fritscher, P. Vela, P. Mitchell, A. Tannenbaum, Interactive medical image segmentation using PDE control of active contours, *IEEE Trans. Med. Imag.* 32 (11) (2013) 2127–2139.
- [19] M.S. Jadin, S. Taib, Recent progress in diagnosing the reliability of electrical equipment by using infrared thermography, *Infrared Phys. Technol.* 55 (4) (2012) 236–245.
- [20] M. Etehadtavakol, S. Sadri, E.Y.K. Ng, Application of K- and fuzzy c-means for color segmentation of thermal infrared breast images, *J. Med. Syst.* 34 (1) (2008) 35–42.
- [21] U. Snehalatha, M. Anburajan, V. Sowmiya, B. Venkatraman, M. Menaka, Automated hand thermal image segmentation and feature extraction in the evaluation of rheumatoid arthritis, *Proc. Inst. Mech. Eng. [H]* 229 (4) (2015) 319–331.
- [22] S. Shahari, A. Wakankar, Color analysis of thermograms for breast cancer detection, 2015 International Conference on Industrial Instrumentation and Control (IIC). (2015). <http://doi.org/10.1109/iic.2015.7151001>.
- [23] M. Etehadtavakol, E. Naag, C. Lucas, S. Sadri, Fuzzy C means segmentation and fractal analysis of the benign and malignant breast thermograms, *Medi. Infrared Imag.* (2012) 1–20.
- [24] M. Etehadtavakol, V. Chandran, E. Ng, R. Kafieh, Breast cancer detection from thermal images using bispectral invariant features, *Int. J. Therm. Sci.* 69 (2013) 21–36.
- [25] A. Hoover, G. Jean-Baptiste, X. Jiang, P. Flynn, H. Bunke, D. Goldgof, K. Bowyer, D. Eggert, A. Fitzgibbon, R. Fisher, An experimental comparison of range image segmentation algorithms, *IEEE Trans. Pattern Anal. Mach. Intell.* 18 (7) (1996) 673–689.
- [26] M. Belgiu, L. Drăguț, Comparing supervised and unsupervised multiresolution segmentation approaches for extracting buildings from very high resolution imagery, *ISPRS J. Photogramm. Remote Sens.* 96 (2014) 67–75.
- [27] R. Adams, L. Bischof, Seeded region growing, *IEEE Trans. Pattern Anal. Mach. Intell.* 16 (6) (Jun 1994) 641–647.
- [28] N. Shareef, D. Wang, R. Yagel, Segmentation of medical images using LEGION, *IEEE Trans. Med. Imaging* 18 (1) (1999) 74–91.
- [29] E. Oliver, J. Ruiz, S. She, J. Wang, The Software Architecture of the GIMP (2006).
- [30] A. Farag, L. Lu, H.R. Roth, J. Liu, E. Turkbey, R.M. Summers, A bottom-up approach for pancreas segmentation using cascaded superpixels and (Deep) image patch labeling, *IEEE Trans. Image Process.* 26 (1) (2017) 386–399.
- [31] L. Bi, J. Kim, A. Kumar, M. Fulham, D. Feng, Stacked fully convolutional networks with multi-channel learning: application to medical image segmentation, *The Visual Computer.* 33 (2017) 1061–1071.
- [32] R.H.H.M. Philipsen, P. Maduskar, L. Hogeweg, J. Melendez, C.I. Sanchez, B.V. Ginneken, Localized energy-based normalization of medical images: application to chest radiography, *IEEE Trans. Medi. Imag.* 34 (9) (2015) 1965–1975.
- [33] P. Ghamisi, M.S. Couceiro, F.M.L. Martins, J.A. Benediktsson, Multilevel image segmentation based on fractional-order darwinian particle swarm optimization, *IEEE Trans. Geosci. Remote Sens.* 52 (5) (2014) 2382–2394.
- [34] J. Chiang, S. Birla, M. Bedoya, D. Jones, J. Subbiah, C.L. Brace, Modeling and validation of microwave ablations with internal vaporization, *IEEE Trans. Biomed. Eng.* 62 (2) (Feb. 2015) 657–663.
- [35] A.R. Sadri, M. Zekri, S. Sadri, N. Gheissari, M. Mokhtari, F. Kolahdouzan, Segmentation of dermoscopy images using wavelet networks, *IEEE Trans. Biomed. Eng.* 60 (4) (April 2013) 1134–1141.
- [36] S. Budzan, R.W.Y.Ż. Golik, Remarks on noise removal in infrared images, *Measur. Autom. Monitoring* 61 (6) (2015) 187–190 Poland.